IN SITU EFFECTIVE DIFFUSION COEFFICIENT PROFILES IN BIOFILMS USING PULSED FIELD GRADIENT-NUCLEAR MAGNETIC RESONANCE (PFG-NMR)

By

RYAN SCOTT RENSLOW

A thesis submitted in partial fulfillment of
the requirements for the degree of

MASTERS OF SCIENCE IN CHEMICAL ENGINEERING

WASHINGTON STATE UNIVERSITY
Department of Chemical Engineering

DECEMBER 2009

To the Faculty of Washington State University:

The members of the Committee appointed to examine the thesis of RYAN S RENSLOW find it satisfactory and recommend that it be accepted.

_____

Haluk Beyenal, Ph.D., Chair

_____

Dr. Cornelius Ivory, Ph.D.

_____

Dr. Paul Majors, Ph.D.

Acknowledgements

I would like to thank Dr. Haluk Beyenal for his enormous support, teaching, and encouragement over the past 3 years that I have known him. He has pushed me and helped me to excel in ways that I could not have done without him. I also want to thank Dr. Paul Majors who taught me the wonder and joy of NMR research. We have had many good times working together at PNNL and I look forward to every time I can travel to Richland, WA to work with him again. Dr. Neil Ivory was my first advisor at WSU. Without him I probably would not be a graduate student right now. It is he who opened my eyes to a possible career in academia and gave me my first taste of university research. Thank you!

Finally I would like to thank my family. My wife, Amanda, is my biggest supporter and the love of my life. Her hard work ethic has helped me to push myself, and her love has given me strength when things seem overwhelming. Thank you mom and dad for your uplifting words, your inspiration to work hard, and your huge financial support for my undergraduate education. Truly, without you, I would not be where I am.

This research was supported by the Office of Science (BER), U.S. Department of Energy, Grant No. DE-FG02-08ER64560. The custom-built NMR microscopy and biofilm reactor hardware development was supported by NIH (NIDCR) R21 DE017232. The work was performed in the Environmental Molecular Sciences Laboratory (a national scientific user facility sponsored by the DOE Biological and Environmental Research) located at the Pacific Northwest National Laboratory and operated for DOE by Battelle. Special thanks to the NIH Training Grant T32-GM008336, which helped fund Ryan Renslow during the project.

IN SITU EFFECTIVE DIFFUSION COEFFICIENT PROFILES IN BIOFILMS USING PULSED FIELD GRADIENT-NUCLEAR MAGNETIC RESONANCE (PFG-NMR)

Abstract

by Ryan Scott Renslow, M.S.
Washington State University
December 2009

Chair: Haluk Beyenal

Diffusive mass transfer in biofilms is characterized by an effective diffusion coefficient. It is well-documented that effective diffusion coefficients vary by location in the biofilms. The literature studies are currently dominated by effective diffusion coefficient measurements for distinct cell clusters or in stratified layers of the biofilms showing this variation. Regardless of whether distinct cell clusters or surface averaging methods are used, the position-dependent measurements of effective diffusion coefficients are 1) invasive to the biofilm, 2) performed under unnatural conditions, 3) at the expense of killing cells, and/or 4) spatially restricted to only certain regions of the biofilm. Invasive measurements can lead to inaccurate results and prohibit further (time-dependent) measurements of biofilms which are important for mathematical modeling of biofilms. In this study we measured *in situ* effective diffusion coefficients in biofilms. Our goals were 1) to measure effective diffusion coefficients of water in live biofilms, 2) to monitor how the effective diffusion coefficients change in biofilms over time, 3) to quantify how heterogeneity of biofilms varies by age and depth, and 4) to correlate biofilm structure with effective diffusion coefficients in biofilms. We measured 2-dimensional effective diffusion coefficient maps in *Shewanella oneidensis* biofilms and generated 1-dimensional surface-averaged effective diffusion coefficient profiles using PFG-NMR methods. All the results are

presented as relative surface-averaged effective diffusion coefficients ($D_{rs)}$. We found that 1) D_{rs} profiles varied for biofilms of differing ages, 2) D_{rs} profiles changed with time and generally decreased with time, 3) all the biofilms we have used showed very similar D_{rs} profiles near the top of the biofilm, 4) D_{rs} profiles near the bottom of the biofilm were different for each biofilm, 5) heterogeneity increased near the bottom of the biofilms, and 6) biofilm heterogeneity increased with age.

Table of Contents

List of Tables

List of Figures

Chapter 1

Introduction

Mass transfer inside the biofilms occurs through both advection, via tortuous channels and pores, and diffusion (de Beer et al. 1994). In most biofilms, diffusive mass transfer dominates (Beuling et al. 1998; Beyenal and Lewandowski 2007; Phoenix and Holmes 2008; Xia et al. 1998). The diffusive mass transfer in biofilms is characterized by the effective diffusion coefficient (D_e) (IUPAC 1997), which is also known as effective diffusivity (Beyenal and Lewandowski 2001; Beyenal and Lewandowski 2002; Beyenal et al. 1998; de Beer et al. 1997; Fu et al. 1994; Zhang and Bishop 1994). Despite the heterogeneous morphology of biofilms, effective diffusion coefficients have been assumed to be constant throughout the biofilm in mathematical models describing biofilm activity and behavior. This is mainly motivated from experimentally measured average effective diffusion coefficients for entire biofilms (Converti et al. 1996; Stewart 1998; Zhang et al. 1998). However, experimental evidence suggests that effective diffusion coefficients are position-dependent and the constant coefficient assumption needs to be modified.

Several researchers have measured effective diffusion coefficients in distinct cell clusters. For example, Lawrence et al. (1994) used fluorescence recovery after photobleaching (FRAP) with scanning confocal laser microscopy (SCLM) to measure effective diffusion coefficients in *Pseudomonas* and mixed-species biofilms. Similar methods were used by De Beer et al. (1997) for determining effective diffusion coefficients in spatially distinct cell clusters and interstitial voids of *Klebsiella* and *Pseudomonas* biofilms. Bryers and Drummond (1998) used layered horizontal FRAP scans to determine volume-averaged effective diffusion coefficients for dextran

and to distinguish biofilm regions with differing densities. More recently, effective diffusion coefficients of fluorescently tagged daptomycin were measured in *Staphylococcus epidermidis* biofilm cell clusters using SCLM (Stewart et al. 2009).

Other researchers measured variations of effective diffusion coefficients in stratified layers of biofilms. In this type of technique, effective diffusion coefficients are calculated for 2-dimensional parallel slices through the biofilm. These measurements yield surface-averaged effective diffusion coefficients (D_{es}). The advantage of these methods is their capability of producing 1-dimensional diffusion coefficient profiles through the depth of the biofilm. Bishop et al. (1995) used a microtome to section frozen biofilms into 10-20 μm parallel layers and calculated D_{es} from the measured structural properties of each layer and found that the effective diffusion coefficients decreased toward the bottom of the biofilm. This technique unavoidably kills the biofilm and damages its structure. Beyenal et al. (1998) averaged the diffusion coefficients of ferricyanide on 225 μm x 225 μm slices through several biofilms. This technique requires the use of potassium ferricyanide, which deactivates the biofilms, and a microelectrode that measures ferricyanide flux. Although this method is quite successful at measuring local effective diffusion coefficients at micron level resolution, it cannot not be used to measure local effective diffusion coefficients near the bottom of the biofilm (0-60 μm from the bottom) due to the mass transfer limitations around the microelectrode tip when near a solid surface.

Regardless of whether distinct cell cluster or surface averaging methods are used, the position-dependent measurements of effective diffusion coefficients are 1) invasive to the biofilm, 2) performed under unnatural conditions, 3) at the expense of killing cells, and/or 4) spatially restricted to only certain regions of the biofilm. Invasive measurements can lead to

inaccurate results and prohibit further (time-dependent) measurements of biofilms which are important for mathematical modeling of biofilms. There is a need to measure diffusive properties of biofilms *in situ* and without affecting biofilm structure or metabolism.

Pulsed field gradient-nuclear magnetic resonance (PFG-NMR) is a noninvasive technique that overcomes limitations of the present methods for measuring effective diffusion coefficients in biofilms. Nuclear magnetic resonance (NMR) is a sensitive tool for displacement studies that uses the nuclear magnetic spin properties of nuclei (typically ^{1}H in water). The effects of diffusion upon NMR signals in liquids have been recognized since its inception over sixty years ago (Bloembergen et al. 1948). Several years later, pulsed field gradient NMR methods were developed to quantitatively measure molecular diffusion rates (Stejskal and Tanner 1965). Today, PFG-NMR is used to measure relative stochastic (Callaghan et al. 1999) and coherent (Caprihan et al. 1990) fluid displacement and can provide directional, including full 3D tensor, information in optically opaque samples without the use of tracers. One distinct advantage of using NMR in transport studies, is that it readily combines with NMR imaging (MRI) and microscopy (μMRI) methods, enabling the spatial mapping of fluid transport.

To measure diffusion using NMR, the sample is subjected to a series of pulsed magnetic field gradients (PFG) that encode each hydrogen atom's displacement into its relative signal phase. This displacement information is preserved as the vector sum of all spins within the volume of measurement. The signal attenuation effects of molecular diffusion are described by the Bloch-Torrey differential equation for transverse magnetization in the presence of a magnetic field gradient (Torrey 1956). The expression for NMR signal attenuation due to diffusion is given by

$$\ln\left(\frac{M}{M_0}\right) = -bD \qquad \text{Equation 1}$$

where M is the observed NMR signal intensity, M_0 is the signal intensity in the absence of gradients, D is the diffusion coefficient, and b is the b-factor (Le Bihan 1990). The b-factor, or the diffusion-weighting factor, is dependent upon the pulse gradient width (δ), the diffusion time interval (Δ), and the strength of the applied gradient. Thus by measuring the signal of a sample for a variety of b-factors, it is possible to solve for D in Equation 1. Furthermore, because the NMR signal is spatially-dependent under the presence of a gradient magnetic field, it is possible to obtain spatially resolved diffusion coefficient measurements.

PFG-NMR methods have been used to measure effective diffusion coefficients in biofilms and other heterogeneous systems. Beuling et al. (1998) used PFG-NMR to measure the diffusion of water in both natural and artificial biofilms. Vogt et al. (2000) employed a combination of bulk-water suppression and fitting the diffusion curves of the individual spectral lines to measure the D_e of three distinct water environments and unidentified chemical components in *Pseudomonas aeruginosa* biofilms by PFG-NMR. In both of these studies, the biofilms were not kept in life-sustaining conditions and measurements were not spatially resolved. Wieland et al. (2001) used both a pulsed field gradient Carr-Purcell-Meiboom-Gill (PFG CPMG) sequence (van Dusschoten et al. 1996) and a pulsed field gradient turbo spin echo (PFG TSE) sequence (Scheenen et al. 1998) to compare 2D diffusion coefficient maps with 2D water density maps of natural microbial mats and to generate diffusion coefficient profiles through the depth of the mats. This study demonstrated that NMR is a powerful biofilm research

tool capable of noninvasively measuring spatially resolved diffusion coefficients. Manz et al. (2003) used PFG-NMR to study the effects of biofilm structure on local fluid velocity. Similarly, PFG-NMR was used by Seymour et al. (2007) to study velocity and transport processes in a biofouled polystyrene-bead packed column. Phoenix and Holmes (2008) took local surface-averaged diffusion coefficient measurements of an un-sustained phototrophic biofilm through PFG-NMR. They averaged the diffusion coefficients on 1 mm x 26 mm slices to create a D_{es} profile through the biofilm. The studied voxels were larger than most natural biofilms. All of these studies showed the wide array of applications and the power of using PFG-NMR for noninvasive biofilm mass transfer studies.

Recently McLean et al., (2008b) showed the possibility of measuring *in situ* effective diffusion coefficients of water in biofilms at the microscale using PFG-NMR imaging. In this study we extended their work and measured *in situ* effective diffusion coefficients in biofilms. The goals were 1) to measure effective diffusion coefficients of water in live biofilms, 2) to monitor how the effective diffusion coefficient changes in biofilms by time, 3) to quantify how heterogeneity of biofilms varies by age and depth, and 4) to correlate biofilm structure with effective diffusion coefficients in biofilms. Two-dimensional effective diffusion coefficient maps in *Shewanella oneidensis* biofilms were measured using PFG-NMR imaging and generated 1-dimensional surface-averaged effective diffusion coefficient profiles. All the results are presented as relative effective diffusion coefficients.

Materials and methods

Reactor to grow biofilms

The biofilms were grown using a modified constant depth film fermenter (CDFF) based on the Wimpenny design (Peters and Wimpenny 1988). The CDFF consisted of a rotating turntable which held fifteen polytetrafluoroethylene (Teflon®) pans located flush around its rim. Each pan contained five cylindrical sample wells (5 mm in diameter each) holding Teflon® plugs. Planar no. 1 glass cover slips (BellCo Glass, Vineland, NJ), 5 mm in diameter and 160 μm thick, were placed on top of the Teflon® plugs and were recessed to a depth of 400 μm using a custom tool. These glass discs were the substratum for biofilm formation. Inoculation and growth medium were introduced through ports located at the top of the CDFF. Air inlet and sample taking ports were also located at the top of the CDFF. Effluent exited from the bottom of the CDFF. Two Teflon® blades, situated above the rotating turntable, sheared the plate surface removing excess biomass to control the depth of the developing biofilm. The medium was dripped onto the turntable pans from a height of 15 mm directly in front of one of the blades. The entire turntable was enclosed in a glass cylinder which was sealed by the top and bottom stainless steel plates.

Growing the biofilms

Biofilms of *Shewanella oneidensis* strain MR-1 were used for this study. Inoculum was prepared by adding 1 mL stock *S. oneidensis* culture to 100 ml (20 g/L) lysogeny broth and allowed to grow for 24 hours under shaking conditions at 30 °C. Approximately 50 mL of the inoculum was pumped at 0.3 mL/min into a clean and autoclave sterilized CDFF. The rotation

rate of the turntable was 8 rpm at all times except directly after inoculation, during which the culture feed and the turntable rotation were stopped for 1 hour to allow for cell attachment. After inoculation, feed of sterile chemically defined minimal medium (see Table 1, slightly modified from McLean et al. (2008a)) was pumped in at 0.3 mL/min. The medium was designed to be compatible with NMR measurements: paramagnetic metal salts were used in tolerably low concentrations and viscosity-enhancing agents such as protein digests were avoided. The CDFF was operated in an incubator at 30 °C. The pressure within the CDFF was kept at equilibrium with filtered (0.2 μm) atmospheric air, therefore ambient oxygen concentrations were maintained at all times. Normal growth conditions were continued after inoculation until the biofilm samples were harvested and aseptically collected through the sample port and transferred to the NMR.

Biofilms were allowed to grow for predetermined times (4 days, 8 days, and 10 days) and then removed from the CDFF. To present results more clearly, time 0 h was designated as the time that each biofilm was transferred into the NMR and the first proton NMR spectrum was collected. From time zero, the biofilms were grown in the NMR from 1 to 6 days.

Table 1. Minimal medium and stock solution compositions.

Chemical	Vendor/Cat#	Concentration in final medium
Minimal medium for *S. oneidensis* MR-1*		
Ammonium Chloride	Sigma A-5666	28.04 mM
Sodium Fumarate dibasic	Sigma F-1506	35 mM
PIPES Buffer	Sigma P-1851	3 mM
Potassium Chloride	Sigma P-4504	1.34 mM
Sodium Chloride	Fisher S271-3	30 mM
Sodium Hydroxide	Sigma S-5881	7.5 mM
Sodium Lactate syrup, 60% (wt/wt)	Sigma L-1375	25.4 mM
Sodium Phosphate monobasic	Sigma S-9638	4.35 mM
Calcium Chloride dihydrate	Sigma C-3881	0.68 mM
Amino acid solution, 100X Stock		See below
Minerals solution, 100X stock		See below
Vitamins solution, 100X stock		See below
Amino Acid Solution, 100X stock*		
DL-serine	Sigma S-4375	2 mg/mL
L-Arginine	Sigma A-3909	2 mg/mL
L-Glutamic Acid	Sigma G-1251	2 mg/mL
Mineral Solution, 100X stock*		
Aluminum potassium disulfate dodecahydrate	Sigma A-7167	0.21 µM
Boric acid	Sigma B-6768	1.62 µM
Calcium Chloride dihydrate	Sigma C-3881	6.8 µM
Cobalt Chloride hexahydrate	Sigma C-3169	4.2 µM
Cupric sulfate pentahydrate	Sigma C-6283	0.4 µM
Ferrous sulfate heptahydrate	Sigma F-8633	3.6 µM
Magnesium sulfate heptahydrate	Aldrich 23039-1	121.71 µM
Manganese sulfate monohydrate	Aldrich 22128-7	29.58 µM
Nickel chloride hexahydrate	Sigma N-6136	1.01 µM
Nitrilotriacetic acid (dissolve with NaOH to pH 8)	Sigma N-9877	78.49 µM
Sodium Chloride	Sigma S-3014	171.12 µM
Sodium Molybdate dihydrate	Aldrich 22184-8	1.03 µM
Sodium tungstate	Sigma S-0765	0.76 µM
Zinc Chloride	Sigma Z-3500	9.54 µM
Vitamin Solution, 100X stock*		
B12	Sigma V-2876	0.72 nM
Biotin (d-biotin)	Sigma B-4639	81.87 nM
d-pantothenic Acid, hemicalcium salt	Sigma P-2250	209.82 nM
Folic Acid	Sigma F-7876	45.34 nM
Nicotinic Acid	Sigma N-4126	406.17 nM
p-aminobenzoic acid	Sigma A-9878	364.62 nM
Pyridoxine HCl	Sigma P-9755	486.38 nM
Riboflavin	Sigma R-4500	132.84 nM
Thiamine HCl 1.0 H2O	Sigma T-4625	140.73 nM
Thioctic acid	Sigma T-5625	242.37 nM

*The medium and each stock solution was set to pH 7.0 after all components had been added using NaOH or HCl.

NMR biofilm reactor

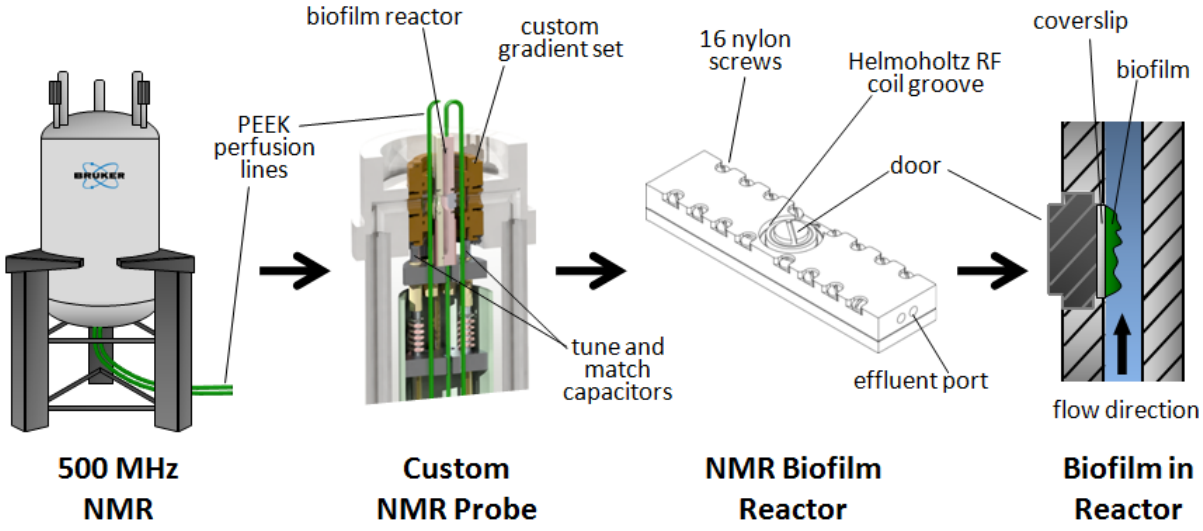

Figure 1. The setup of the NMR biofilm reactor. Starting at the left, the Bruker NMR with perfusion lines entering at the bottom of the bore. Next, the custom NMR probe is shown holding the NMR biofilm reactor. Third from the left, the 3D view of the outside of the NMR biofilm reactor. The two halves of the reactor are held together by 16 nylon screws. The door holds the coverslip in place (parallel to the NMR bore) and seals the reactor from leaking. Finally, at the far right, a cutaway view of the NMR biofilm reactor is shown. The biofilm protrudes into the flow of the medium, which is pumped against gravity.

Each CDFF-grown sample was transferred to a specially designed NMR biofilm reactor constructed from Torlon® polyamide-imide plastic. A single-pass flow system consisted of a medium reservoir bottle, a pulseless dual syringe pump (Pharmacia P-500, Uppsala, Sweden), the NMR biofilm reactor (inside of the NMR magnet), and a waste reservoir bottle connected in series with polyetheretherketone (PEEK) plastic tubing. Drip-isolation tubes were placed upstream of the reactor to minimize microbial growth and avoid back contamination. The reactor was constructed so that the glass cover slip completed one wall of the 4 mm wide flow channel. Consequently, the biofilm protruded into the bulk liquid flow path. Figure 1 shows the NMR biofilm reactor and its location in the NMR probe. The inside dimensions for the chamber were

40 mm long, 4 mm wide, and 2 mm tall, giving a total liquid volume of 320 µL. When installed in the magnet, the coverslip was parallel to the magnet bore and coincident with the Helmholtz radiofrequency detection coil axis. Four 0.762 mm inner diameter PEEK perfusion lines were attached to the chamber parallel to the coverslip, two located at each end.

During all experiments, one input and one output line were used to feed the growth medium. The injection line was run from the pump through the vertical NMR bore against gravity and the effluent line was run outside of the radiofrequency detection coil and the magnetic field gradients back down the bore to a waste collection beaker. Oxygen saturated minimal medium, identical to that used in the CDFF, was pumped through the reactor at 1 mL/h, which resulted in a laminar flow profile (Reynolds number of 0.1). Hydraulic retention time in the reactor was 19.2 minutes (dilution rate of 3.125 h^{-1}). A temperature controlled gas stream delivery unit (FTS Systems, Stone Ridge, NY, USA) maintained a purge of nitrogen gas in the magnet bore and around the sample chamber, keeping the reactor and perfusion lines in the bore at 30 ± 0.2 °C.

NMR measurements

All NMR measurements were performed at 500.44 MHz for protons (^{1}H) using a Bruker Avance digital NMR spectrometer (Bruker Instruments, Billerica, MA, USA) with an 11.7 T, 89 mm vertical bore, actively shielded superconducting magnet. Bruker software TopSpin v1.5 and ParaVision v4.0 imaging software was used to collect and process the data. Measurements included 1) rapid multidirectional NMR imaging to verify correct sample positioning and the absence of gas bubbles, 2) 2-dimensional Fourier transform (2DFT) MRI, and 3) diffusion-

mapping 2DFT MRI. The field of view (FOV) dimensions were 3.84 mm in the biofilm-depth direction and 8.00 mm in the flow direction for both the MRI and diffusion-mapping measurements. 512 complex points were sampled at a rate of 98 Hz in the depth direction with 32 phase-encoding steps for an in-plane resolution of 7.50 by 250 μm. For diffusion mapping, the standard diffusion tensor imaging (DTI) Paravision method (DtiStandard) was employed with a repetition time of 1000 milliseconds, an echo time of 25 milliseconds, and 24 averages. The pulse gradient width (∂) was 2 milliseconds and the diffusion time interval (Δ) was 10 milliseconds. The imaging sequence was repeated with six different diffusion-weighting values (b-factors) of 1, 10, 375, 750, 1125, and 1500 s/mm^2 (aligned with the slice direction, i.e. parallel with the coverslip surface and perpendicular to the flow direction) for a total measurement time of 77 minutes.

The diffusion maps were generated by processing (Gaussian noise filtering followed by fast 2DFT processing) the individual images, then performing a semilogarithmic analysis of the b-factor-dependent intensity value of each image pixel above a preset noise threshold. In accord with Equation 1, the calculated diffusion coefficients are assigned as pixel values of the resulting 2D quantitative effective diffusion coefficient (D_e) map.

Calculations for diffusion coefficient profiles

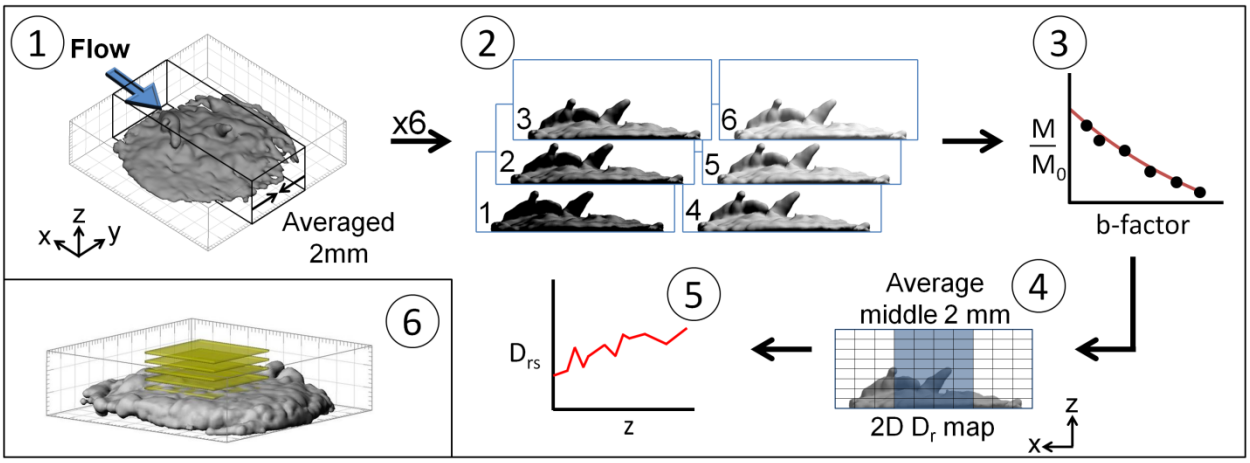

Figure 2. The steps to obtain a diffusion coefficient profile: 1) The NMR measurements experimentally provided averaging in the y direction by selecting a 2 mm thick slab aligned normal to that direction, and spatially resolving in the x (phase encode) and z directions. 2) A series of six diffusion-weighted 2D images were collected, each having a unique b-factor value. 3) A semilogarithmic fit for each pixel location was performed to find the diffusion coefficient value for each pixel location. 4) The result was a 2D (x-z) map of effective diffusion coefficients (where the diffusion rate was modulated by spatial hindrance due to the presence of biomass). 5) To obtain the depth-resolved surface average effective diffusion coefficient profiles, image pixels corresponding with the middle 2 mm of the sample were averaged along the x axis. 6) A 3D MRI image of the 10-day old biofilm and yellow slices showing the final shape and location of the apparent surface averaging slices used to produce the diffusion coefficient profiles.

Figure 2 schematically describes the calculations required to generate the diffusion coefficient profiles. The direct measurement from the NMR results in a 2D D_e map. The middle 2 mm of the biofilm are averaged along the x-direction to create a z-dependent D_e profile. Surface-averaged relative effective diffusion coefficient (D_{rs}) profiles were calculated by dividing the results by the bulk liquid diffusion coefficient (D_{aq}). The expression for surface-averaged relative effective diffusion coefficient is given by:

$$D_{rs} = \frac{D_{es}}{D_{aq}} \qquad \text{Equation 2}$$

Each data point in the profile thus represents the average of the effective relative diffusion coefficients across a 2 mm x 2 mm surface that is concentric with the coverslip. Figure 2 part 6 shows a volume filled 3D MRI of the 10-day old biofilm with slices depicting the apparent location of the surface averaging calculations. MRI data was used to determine the location of biofilm interfaces, including the top and bottom of the biofilm. Imaris v6.1.5 image rendering software (Bitplane, Zürich, Switzerland) was used to process the 3D data. All other calculations were performed on Excel 2007 (Microsoft, Redmond, Washington, USA).

Results and discussions

Figure 3 shows a typical 2D relative effective diffusion coefficient (D_r) map we obtained using PFG-NMR with selected features of the biofilm and reactor. In this typical example map, the biofilm was 10-day old. This map corresponds to step 4 in Figure 2. Maps similar to Figure 3 were used to generate the D_{rs} profiles shown in the following sections.

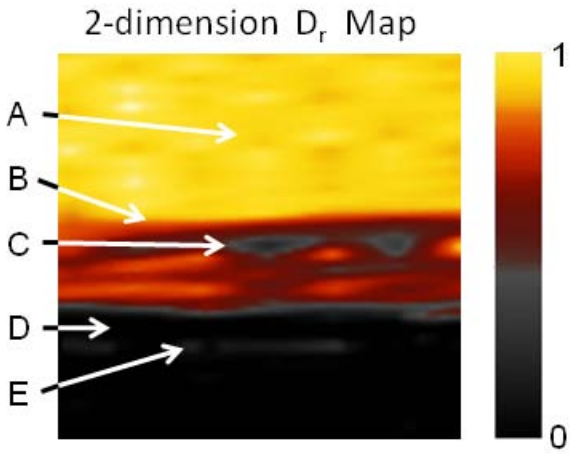

Figure 3. A typical 2D relative effective diffusion coefficient (D_r) map of the NMR biofilm reactor obtained by PFG-NMR. The middle 2 mm of the 10-day old biofilm are shown here. A) The bulk liquid (yellow) flowing above the biofilm; B) the top of the biofilm (yellow/red interface); C) a low diffusion region in the biofilm (gray); D) the coverslip that supports the biofilm (black); and E) a thin layer of water trapped between the coverslip and the reactor door.

D_{rs} changes with distance and biofilm age

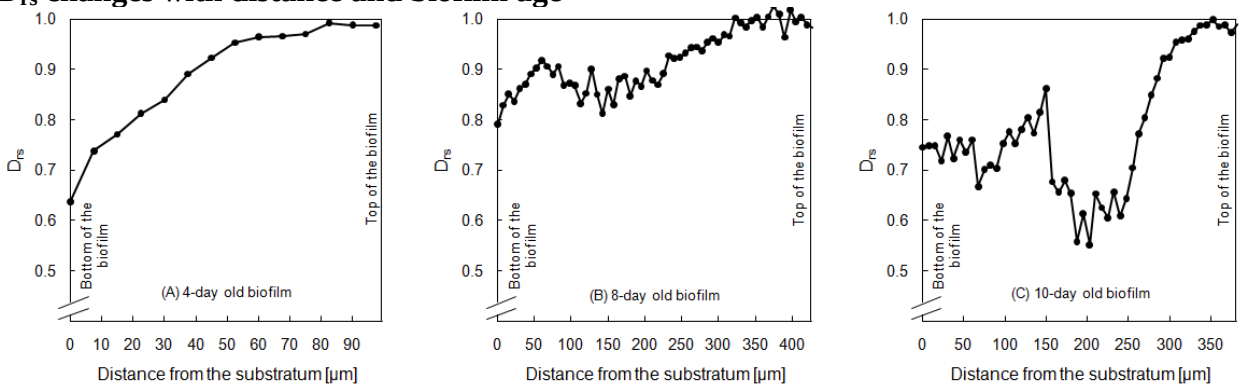

Figure 4. *In situ* D_{rs} profiles in three *S. oneidensis* biofilms shown from the bottom to the top of the biofilms. A) 4-day old biofilm; B) 8-day old biofilm; C) 10-day old biofilm. The biofilms at different ages showed different profiles.

Figure 4 shows the variation of D_{rs} by distance for biofilms which were harvested from the CDFF reactor at different ages: 4 days, 8 days, and 10 days. The D_{rs} is around 1 near the biofilm surface and in the bulk liquid for all biofilms. For the 4-day old biofilm, the D_{rs}

decreases nearly linearly to a value of 0.65 at the bottom of the biofilm. Similar linear profiles were also observed by Beyenal et al. (1998) for 5-day old mixed species biofilms. The two older biofilms used in our experiments demonstrated different profiles where the D_{rs} decreases for approximately 200 μm and then begins to increase irregularly near the bottom of the biofilms. The 8-day old biofilm had a D_{rs} local minimum near the middle of the biofilm, and the D_{rs} subsequently rose again near the bottom. The 10-day old biofilm showed an even more drastic drop in the middle. For all biofilms, the profiles decrease overall from the top of the biofilm to the bottom. The average relative effective diffusion coefficients (D_r, which is D_{rs} averaged across the entire profile) are 0.89, 0.92, and 0.78 for the 4-day old, 8-day old, and 10-day old biofilms respectively.

The link between biofilm density and diffusion coefficients can be approximated by the following expression (Beyenal and Lewandowski 2005; Beyenal and Lewandowski 2007; Fan et al. 1990):

$$X = -38.856 + 38.976(D_{rs})^{-0.7782} \qquad \text{Equation 3}$$

Equation 3 shows biofilm density is inversely related to diffusion coefficients, and thus we assume that increasing diffusion coefficients represent decreasing density in our biofilms. When we compare the diffusion coefficient profile in Figure 4A with the other profiles, we noticed that the middle of the biofilm becomes denser as the biofilm age increases due to the decreased effective diffusion coefficient. For prolonged times (more than 8 days) of biofilm growth, less substrate is delivered to the bottom of the biofilm and the cells near bottom starve because of

diffusion limitations. This changes their phenotype. This phenotype change due to starvation may lead to cell cluster hollowing ("seeding dispersal") which has been observed by several researchers. For example, Stewart et al. (2007) grew *Staphylococcus epidermidis* biofilms and observed hollowing in 2-day old biofilms. One possible explanation given by Stewart et al. for this phenomenon is nutrient starvation in the depths of the biofilm. Similarly, McLean et al. (2008a) monitored the hollowing effect in *S. oneidensis* MR-1, and mass transfer influences (both build-up or limitations of metabolites) were discussed as a possible cause. We should note that the top of the cell clusters were detached at the end of the hollowing effect observed by Stewart et al. and McLean et al. However, in our case, the biofilm was still intact at the end of experimentation, but with decreasing cell density near the bottom of the biofilm.

D_{rs} near the surface of the biofilms

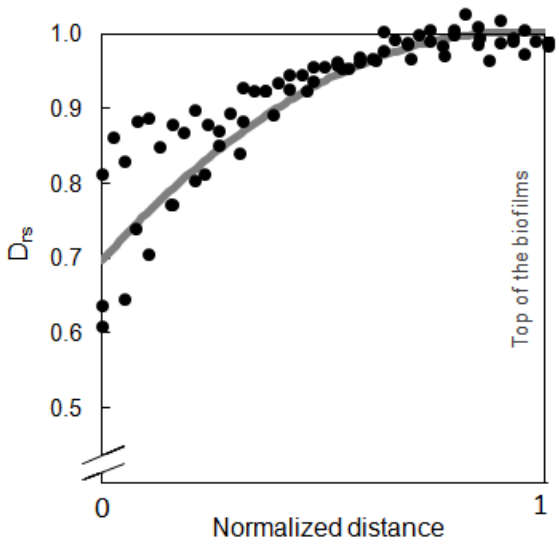

Figure 5. D_{rs} data points near the top of each biofilm. Data points are taken from the local minimum in the middle of each biofilm (normalized to 0) to the top of each biofilm (normalized to 1). An exponential decay fit to the data is shown in gray.

Figure 5 shows the D_{rs} profiles between the surface of the biofilm and the local minimum found in the middle of each biofilm, except the 4-day old biofilm, in which the entire profile is shown. Figure 5 qualitatively shows that all biofilms in our experiments had comparable smoothly decreasing and consistently concave down profiles near the top regardless of their age. We believe this is mostly because of the activity of the cells near the surface. Our research group repeatedly measured activity of biofilms using a dissolved oxygen microelectrode. We found that on average, oxygen is consumed in the first 100 μm from the top of the biofilm. It appears that when biofilms have similar activity, they have very similar diffusion coefficient profiles.

The mean trend for all biofilms is shown as the gray trend line, where the value at the bulk liquid interface is set as 1. It is important to note that the bulk liquid interface of all biofilms starts with a D_{rs} value of 1 (± 0.02) and that the profiles have a shallow slope for the initial third of each biofilm. This is due to both the nature of the biofilm surface and the surface average processing. Liquid interfaces of biofilms are highly mottled regions with pockets, "fingers", and a rough morphology. Surface averaging this interfacial region levels out the heterogeneity and results in a smooth and gradually decreasing profile. Deeper into the biofilm matrix, there are less pockets of water, more of the matrix is filled with EPS and cells, and the rate of mass transfer drops.

A smooth profile like Figure 5 is commonly used in biofilm modeling and may be appropriate for modeling young biofilms. However, for modeling older biofilms or when modeling biofilms over time, it appears that heterogeneity and irregular profiles should be considered. Biofilm modelers should take into account that biofilms can have variable densities and grow non-linearly. Certain regions of the biofilm demonstrate higher diffusion limitations,

receive limited amount of nutrients, and complex mass transfer can dominate. This can lead to the complex profiles shown in Figure 4.

D_{rs} changes by time

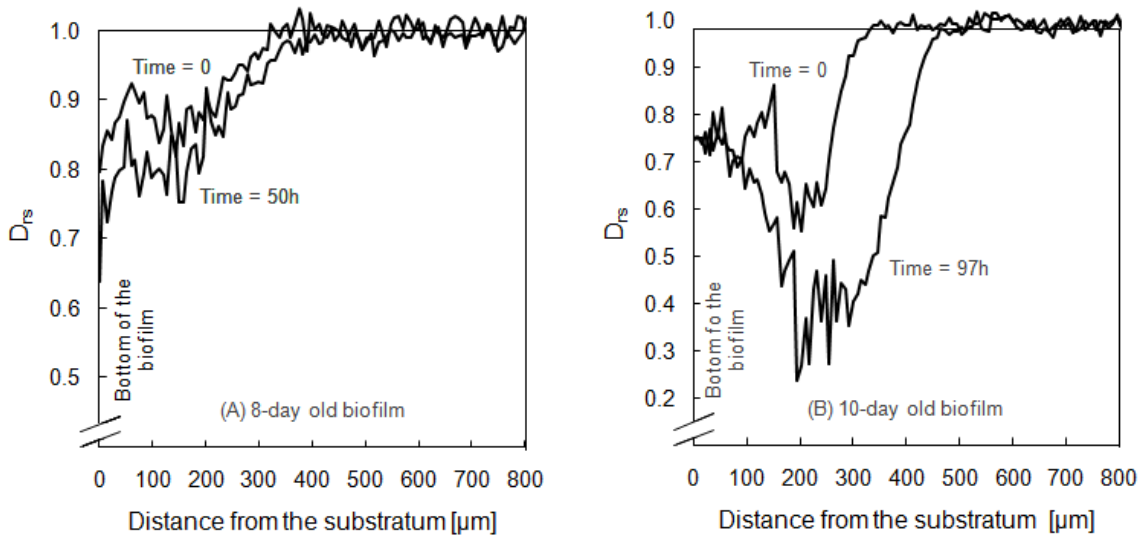

Figure 6. D_{rs} profile of the 8-day old biofilm at 0 hours and 50 hours, and the 10-day old biofilm at 0 hours and 97 hours.

Since we observed different D_{rs} profiles for biofilms harvested at different ages, we monitored D_{rs} variation by time for the same biofilms while the biofilms continued to grow in the NMR reactor. The time-lapsed profiles are shown in Figure 6. Figure 6 compares the profiles of the 8-day old biofilm and the 10-day old biofilm, each at two different times. Note that the scale reaches beyond the bulk liquid interface to show biofilm growth. The D_{rs} profiles changed over time. Both biofilms became less diffusible with time and biofilm thickness increased, especially for the 10-day old biofilm. It is possible to see the bulk liquid interface advance from around 350 μm to 450 μm. The 10-day old biofilm had a significant change near the middle of the biofilm as

the D_{rs} dropped from 0.6 to 0.3. We believe that the density in this region is increasing, causing a restriction in mass transfer through the biofilm. This is possibly due to bacterial growth, cell multiplication, and/or increased EPS formation.

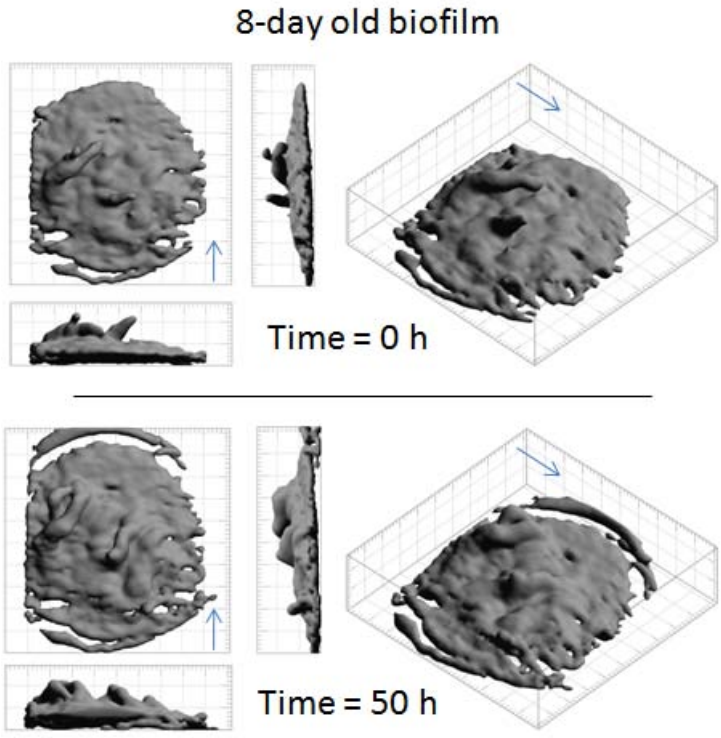

Figure 7. 3D MRI images of the 8-day old biofilm at 0 hours and 50 hours. The blue arrows show the direction of fluid flow.

Figure 7 shows the variation of biofilm structure in 3-dimensions over time for the 8-day old biofilm. As time progressed, the biofilm structure changed. For example, it is possible to see protruding "fingers" present at time 0 h, but at time 50 h the "fingers" are attached to the bulk biomass. Also, many regions of the biofilm appear to be thicker and more filled-in at time 50 h. At the biofilm surface, cell clusters do not appear to simply grow uniformly in all directions.

This type of non-uniform growth is common in recent biofilm models (Ebrahimi et al. 2005; Kreft et al. 2001; Picioreanu et al. 1998; Picioreanu et al. 2000; Xavier and Foster 2007). Our experimental data supports the idea that the growth of the biofilm in 3-dimension is not as simple as consistent and even expansion. As we demonstrated earlier in Figure 6, internal changes of the structure were also very pronounced. These results collectively demonstrate that physical changes that affect mass transfer are occurring both internally through increasing density, and externally as the biofilm-liquid interface expands and transforms.

Biofilm heterogeneity

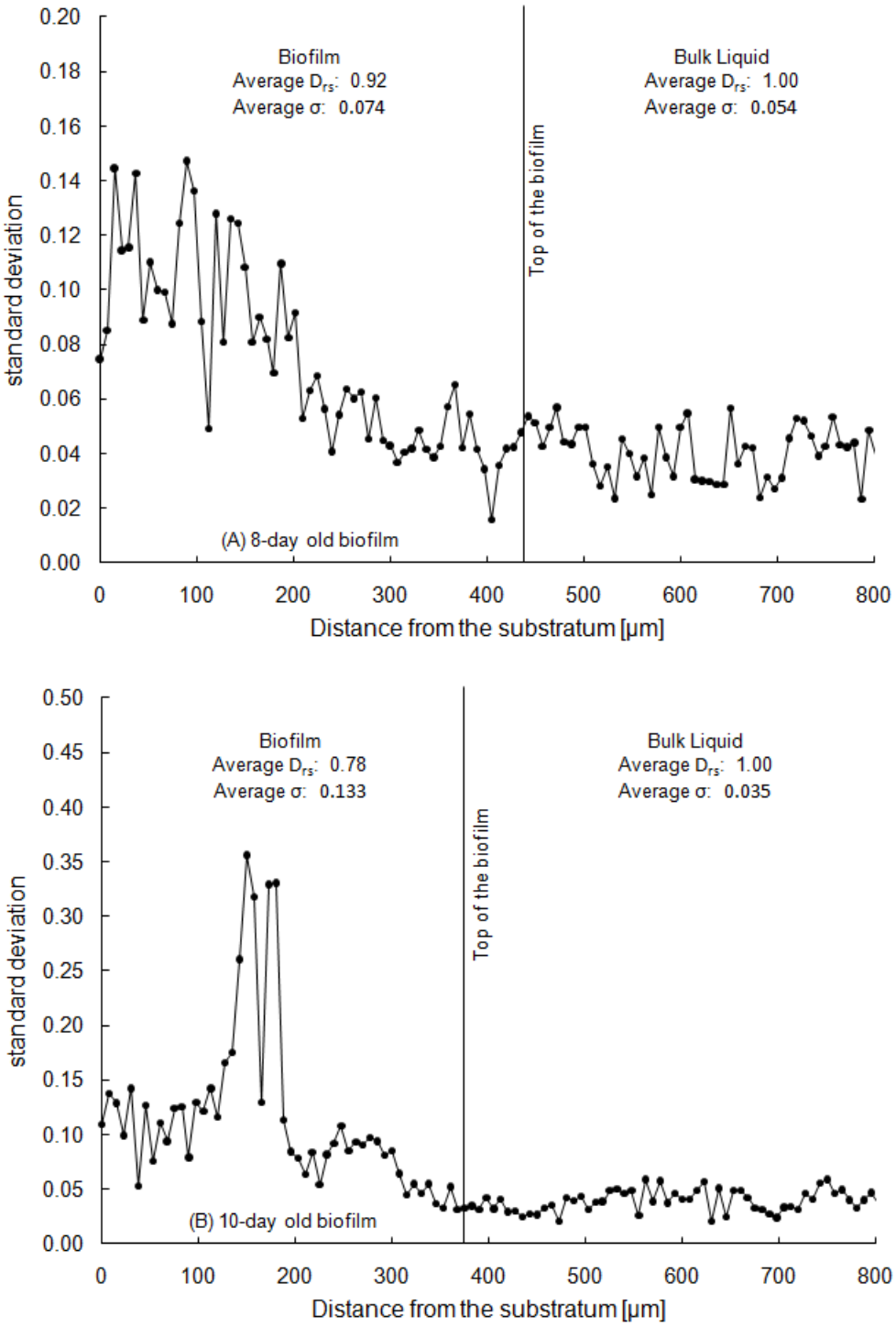

Figure 8. Standard deviation [$m^2 \cdot s^{-1}$] for each D_{rs} data point for the A) 8-day old biofilm and B) 10-day old biofilm.

In Figure 8, standard deviations of each D_{rs} data point as a function of distance are shown for the 8-day old biofilm and the 10-day old biofilm. The average standard deviations are 0.074 and 0.133 for the biofilm section of the 8-day old biofilm and the 10-day old biofilm respectively. Biofilm heterogeneity is generally poorly defined in the literature. It describes variations of a selected parameter or set of parameters. In our work, we used standard deviations of the D_{rs} to quantify local biofilm heterogeneity. The 10-day old biofilm has more heterogeneous regions than the 8-day old biofilm because it has a larger standard deviation in those regions. This aligns with the conclusion from above that heterogeneity increases with biofilm age. The standard deviations increase near the bottom of both biofilms compared to the region near the top of the biofilms. This shows that the bottom of our biofilms are more heterogeneous than near the tops. This makes sense given the smooth D_{rs} trends seen near the top of each biofilm, and the erratic profiles near the substratum.

Figure 8 also displays the average standard deviation in the bulk liquid region up to 800 μm. They are 0.054 for the 8-day old biofilm and 0.035 for the 10-day old biofilm. This region of the sample chamber has a flat D_{rs} profile. However, Beuling et al. (1998) reported slightly higher values.

Table 2 shows the quantitative effective diffusion coefficient values for the bulk liquid. These values were obtained far away from the biofilm, from the region corresponding to 1500-1700 μm away from the substratum, to insure the measurement was not affected by loose cells or biofilm "fingers". D_{aq} ranged from $2.23 \cdot 10^{-9}$ m^2/s to $2.42 \cdot 10^{-9}$ m^2/s. The D_{aq} values we measured are similar to the values obtained by Simpson and Carr (1958), who used NMR at 30 °C, and fall

within the error range that they reported. However, Beuling et al. (1998) reported slightly higher values.

Table 2. Diffusion coefficients for the bulk liquid present above the biofilm for each experiment and literature values. Values at 30 °C are highlighted in gray. Data from Beuling et al. estimated from Figure 3 of their paper (1998).

Experiment	D_{aq} [m^2/s]	Temp [°C]
4-day old biofilm	$2.42 \cdot 10^{-9}$	30
8-day old biofilm	$2.41 \cdot 10^{-9}$	30
10-day old biofilm	$2.25 \cdot 10^{-9}$	30
Beuling et al., 1998	$2.30 \cdot 10^{-9}$	25
Beuling et al., 1998	$2.68 \cdot 10^{-9}$	30
Beuling et al., 1998	$3.10 \cdot 10^{-9}$	35
Simpson and Carr, 1958	$2.13 \cdot 10^{-9}$	25
Simpson and Carr, 1958	$2.46 \cdot 10^{-9}$	30
Simpson and Carr, 1958	$2.79 \cdot 10^{-9}$	35

To attempt to quantify overall heterogeneity (non-local morphological variability) in the biofilms as a function of biofilm age, linear regression (D_{rs} versus z) was performed on each D_{rs} profile and the coefficient of determination (R^2) was calculated for the best-fit linear lines. R^2 can be considered a measure of "goodness of fit" for each profile. An overall homogeneous biofilm will have a flat or linearly smooth diffusion coefficient profile, and conversely a heterogeneous biofilm will have a non-linear profile. The inverse of R^2 is proportional to the variability in the data as the data becomes less linear (increasingly heterogeneous). Therefore, the inverse R^2 value can be used as a way to quantify overall biofilm heterogeneity. A completely homogeneous profile will have an inverse R^2 value of 1. Heterogeneity increases as the inverse R^2 value increases. The inverse R^2 values are 1.16, 1.32, and 2.91 for the 4-day old, 8-day old, and 10-day old biofilms respectively, as shown in

Table **3**. From our definition, the biofilms have increasing heterogeneity with age. This tells us that the density distribution within the biofilms is becoming more spatially erratic as the biofilm age increases.

Table 3. Heterogeneity, as measured by inverse R^2 values, for each D_{rs} profile.

Experiment	D_{rs} profile heterogeneity ($1/R^2$)
4-day old biofilm	1.16
8-day old biofilm	1.32
10-day old biofilm	2.91

D_{rs} and biofilm structure

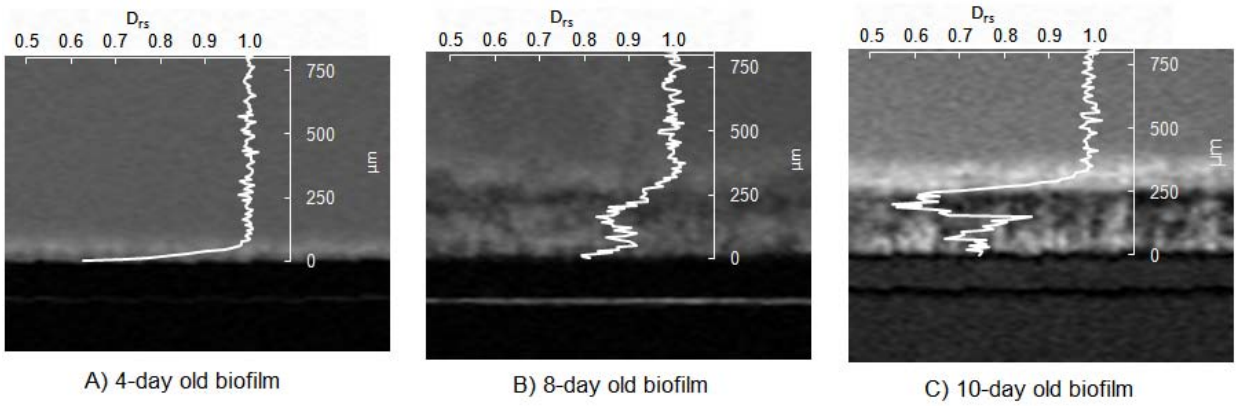

Figure 9. D_{rs} profiles overlaid with the corresponding MRI intensity images of the flow chamber (and biofilms) for the A) 4-day old biofilm, B) 8-day old biofilm, and C) 10-day old biofilm.

To understand how morphology relates to diffusion coefficients, 2D MRI intensity images of each biofilm were captured. Figure 9 shows the MRI intensity images with the corresponding D_{rs} profiles for each biofilm. The MRI region shown matches both size and location of the 2 mm slices used for the D_{rs} profiles. At the bottom of each image, the dark region shows the Torlon® door of the chamber, a thin medium layer, and the coverslip. On the surface

of the coverslip the biofilm is distinguishable from the monochromatic bulk liquid. The middle of these biofilms are much more dense than the regions near the interfaces with the coverslip and the bulk liquid because the middle gives less NMR signal (seen as darker on the MRI). The MRI images in Figure 9 show a bright boundary layer between the biofilm and the bulk liquid with more signal intensity than the bulk liquid. This is a common effect caused by a biofilm surface-enhanced reduction of the T_1 relaxation rate for water in conjunction with local water exchange. Within the interior of the biofilm, reduced signal is usually an indication of excluded water or an increase in solid or gas phase objects (i.e. dense biomas, EPS, bubbles, etc).

Several correlations between the MRI intensity images and the D_{rs} profiles can be seen. One correlation is between the change in the D_{rs} profile and the bulk liquid biofilm interface. Diffusion coefficient measurements could be used to determine the surface of the biofilm in situations where images of the biofilm are not available, and are perhaps more reliable as the boundary-layer relaxation contrast seen in the MRI does not influence the diffusion profiles. A second correlation is observed between the drop in D_{rs} near the middle of the two older biofilms and the low MRI intensity for the same region. This supports our hypothesis that the middle regions of these biofilms are more dense and mass transfer is restricted. In both the 8-day old biofilm and the 10-day old biofilm, the MRI images show evidence for the increase in heterogeneity near the coverslip. Particularly in the 10-day old biofilm, alternating regions and irregularly dispersed pockets of light and dark intensity dominate the bottom of the biofilm, whereas at the top of the biofilm the MRI intensity is fairly constant.

Conclusions

- We have measured in-situ surface-averaged relative effective diffusion coefficient profiles in living biofilms using a non-invasive technique.
- D_{rs} profiles differ from biofilms of differing ages.
- D_{rs} profiles changed with time and generally decreased with time.
- All the biofilms we have used showed very similar D_{rs} profiles near the top of the biofilm.
- D_{rs} profiles near the bottom of the biofilm were different for each biofilm
- Local heterogeneity increased near the bottom of the biofilms.
- Overall biofilm heterogeneity increased with age.

Nomenclature

∂	pulse gradient width (for Dti measurements) [ms]
Δ	diffusion time interval (for Dti measurements) [ms]
σ	standard deviation
b	b-factor [$s \cdot m^{-2}$]
D	diffusion coefficient [$m^2 \cdot s^{-1}$]
D_{aq}	bulk liquid diffusion coefficient [$m^2 \cdot s^{-1}$]
D_e	effective diffusion coefficient [$m^2 \cdot s^{-1}$]
D_r	relative effective diffusion coefficient [dimensionless]
D_{es}	surface averaged effective diffusion coefficient [$m^2 \cdot s^{-1}$]
D_{rs}	surface averaged relative effective diffusion coefficient [dimensionless]
M	observed NMR signal intensity [a.i.]
M_0	NMR signal intensity in the absence of gradients [a.i.]
R^2	coefficient of determination [dimensionless]
X	average biofilm density [$kg \cdot m^{-3}$]

Acronyms

µMRI	micro magnetic resonance imaging (NMR microscopy)
2D	2-dimensional
2DFT	2-dimensional Fourier transform
3D	3-dimensional
a.i.	absolute intensity
CDFF	constant depth film fermenter
Dti	diffusion tensor imaging
EPS	extracellular polymeric substances
FOV	field of view
FRAP	fluorescence recovery after photobleaching
MRI	magnetic resonance imaging (NMR imaging)
NMR	nuclear magnetic resonance
PFG-NMR	pulsed field gradient-nuclear magnetic resonance
SCLM	scanning confocal laser microscopy

References

Beuling EE, van den Heuvel JC, Ottengraf SPP. 2000. Diffusion coefficients of metabolites in active biofilms. Biotechnology and Bioengineering 67(1):53-60.

Beuling EE, van Dusschoten D, Lens P, van den Heuvel JC, Van As H, Ottengraf SPP. 1998. Characterization of the diffusive properties of biofilms using pulsed field gradient-nuclear magnetic resonance. Biotechnology and Bioengineering 60(3):283-291.

Beyenal H, Lewandowski Z. 2001. Mass-transport dynamics, activity, and structure of sulfate-reducing biofilms. Aiche Journal 47(7):1689-1697.

Beyenal H, Lewandowski Z. 2002. Internal and external mass transfer in biofilms grown at various flow velocities. Biotechnology Progress 18(1):55-61.

Beyenal H, Lewandowski Z. 2005. Modeling mass transport and microbial activity in stratified biofilms. Chemical Engineering Science 60(15):4337-4348.

Beyenal H, Lewandowski Z. 2007. Fundamentals of Biofilm Research: CRC.

Beyenal H, Tanyolac A, Lewandowski Z. Measurement of local effective diffusivity in heterogeneous biofilms; 1998. Pergamon-Elsevier Science Ltd. p 171-178.

Bishop PL, Zhang TC, Fu YC. 1995. Effects of biofilm structure, microbial distributions and mass-transport on biodegradation processes. 31:143-152.

Bloembergen N, Purcell EM, Pound RV. 1948. Relaxation Effects in Nuclear Magnetic Resonance Absorption. Physical Review 73(7):679-712.

Bryers JD, Drummond F. 1998. Local macromolecule diffusion coefficients in structurally non-uniform bacterial biofilms using fluorescence recovery after photobleaching (FRAP). Biotechnology and Bioengineering 60(4):462-473.

Callaghan PT, Codd SL, Seymour JD. 1999. Spatial coherence phenomena arising from translational spin motion in gradient spin echo experiments. Concepts in Magnetic Resonance 11(4):181-202.

Caprihan A, Griffey RH, Fukushima E. 1990. Velocity imaging of slow coherent flows using stimulated echoes. Magnetic Resonance in Medicine 15(2):327-333.

Converti A, Casagrande M, deGiovanni M, Rovatti M, DelBorghi M. 1996. Evaluation of glucose diffusion coefficient through cell layers for the kinetic study of an immobilized cell-bioreactor. Chemical Engineering Science 51(7):1023-1026.

de Beer D, Stoodley P, Lewandowski Z. 1994. Liquid flow in heterogeneous biofilms. Biotechnology and Bioengineering 44(5):636-641.

de Beer D, Stoodley P, Lewandowski Z. 1997. Measurement of local diffusion coefficients in biofilms by microinjection and confocal microscopy. Biotechnology and Bioengineering 53(2):151-158.

Ebrahimi S, Picioreanu C, Xavier JB, Kleerebezem R, Kreutzer M, Kapteijn F, Moulijn JA, van Loosdrecht MCM. 2005. Biofilm growth pattern in honeycomb monolith packings: Effect of shear rate and substrate transport limitations. Catalysis Today 105(3-4):448-454.

Fan LS, Leyvaramos R, Wisecarver KD, Zehner BJ. 1990. Diffusion of phenol through a biofilm grown on activated carbon particles in a draft-tube 3-phase fluidized-bed bioreactor. Biotechnology and Bioengineering 35(3):279-286.

Fu YC, Zhang TC, Bishop PL. 1994. Determination of effective oxygen diffusivity in biofilms grown in a completely mixed biodrum reactor. 29:455-462.

IUPAC. 1997. Compendium of Chemical Terminology, 2nd ed. (the "Gold Book"). Oxford: Blackwell Scientific Publications.

Kreft JU, Picioreanu C, Wimpenny JWT, van Loosdrecht MCM. 2001. Individual-based modelling of biofilms. Microbiology-Sgm 147:2897-2912.

Lawrence JR, Wolfaardt GM, Korber DR. 1994. Determination of diffusion-coefficients in biofilms by confocal laser microscopy. Applied and Environmental Microbiology 60(4):1166-1173.

Le Bihan D. 1990. Magnetic-resonance-imaging of perfusion. Magnetic Resonance in Medicine 14:283-292.

Manz B, Volke F, Goll D, Horn H. 2003. Measuring local flow velocities and biofilm structure in biofilm systems with magnetic resonance imaging (MRI). Biotechnology and Bioengineering 84(4):424-432.

McLean JS, Majors PD, Reardon CL, Bilskis CL, Reed SB, Romine MF, Fredrickson JK. 2008a. Investigations of structure and metabolism within Shewanella oneidensis MR-1 biofilms. Journal of Microbiological Methods 74(1):47-56.

McLean JS, Ona ON, Majors PD. 2008b. Correlated biofilm imaging, transport and metabolism measurements via combined nuclear magnetic resonance and confocal microscopy. Isme Journal 2(2):121-131.

Peters AC, Wimpenny JWT. 1988. A constant-depth laboratory model film fermentor. Biotechnology and Bioengineering 32(3):263-270.

Phoenix VR, Holmes WM. 2008. Magnetic resonance imaging of structure, diffusivity, and copper immobilization in a phototrophic biofilm. Applied and Environmental Microbiology 74(15):4934-4943.

Picioreanu C, van Loosdrecht MCM, Heijnen JJ. 1998. Mathematical modeling of biofilm structure with a hybrid differential-discrete cellular automaton approach. Biotechnology and Bioengineering 58(1):101-116.

Picioreanu C, van Loosdrecht MCM, Heijnen JJ. 2000. Effect of diffusive and convective substrate transport on biofilm structure formation: A two-dimensional modeling study. Biotechnology and Bioengineering 69(5):504-515.

Scheenen TWJ, Dusschoten Dv, Jager PAd, As HV. 1998. Fast Spatially Resolved Displacement Imaging in (Bio) Systems. In: Blümler PDP, Blümich PDB, Botto PDR, Fukushima DE, editors. Spatially Resolved Magnetic Resonance: Wiley. p 481-486.

Seymour JD, Gage JP, Codd SL, Gerlach R. 2007. Magnetic resonance microscopy of biofouling induced scale dependent transport in porous media. Advances in Water Resources 30(6-7):1408-1420.

Simpson JH, Carr HY. 1958. Diffusion and Nuclear Spin Relaxation in Water. Physical Review 111(5):1201.

Stejskal EO, Tanner JE. 1965. Spin Diffusion Measurements: Spin Echoes in the Presence of a Time-Dependent Field Gradient. The Journal of Chemical Physics 42(1):288-292.

Stewart PS. 1998. A review of experimental measurements of effective diffusive permeabilities and effective diffusion coefficients in biofilms. Biotechnology and Bioengineering 59(3):261-272.

Stewart PS, Davison WM, Steenbergen JN. 2009. Daptomycin Rapidly Penetrates a Staphylococcus epidermidis Biofilm. Antimicrobial Agents and Chemotherapy 53(8):3505-3507.

Stewart PS, Rani SA, Gjersing E, Codd SL, Zheng Z, Pitts B. 2007. Observations of cell cluster hollowing in Staphylococcus epidermidis biofilms. Letters in Applied Microbiology 44(4):454-457.

Torrey HC. 1956. Bloch Equations with Diffusion Terms. Physical Review 104:563-565.

van Dusschoten D, Moonen CTW, deJager PA, VanAs H. 1996. Unraveling diffusion constants in biological tissue by combining Carr-Purcell-Meiboom-Gill imaging and pulsed field gradient NMR. Magnetic Resonance in Medicine 36(6):907-913.

Vogt M, Flemming HC, Veeman WS. 2000. Diffusion in Pseudomonas aeruginosa biofilms: a pulsed field gradient NMR study. Journal of Biotechnology 77:137-146.

Wieland A, de Beer D, Damgaard LR, Kuhl M, van Dusschote D, Van As H. 2001. Fine-scale measurement of diffusivity in a microbial mat with nuclear magnetic resonance imaging. Limnology and Oceanography 46(2):248-259.

Xavier JB, Foster KR. 2007. Cooperation and conflict in microbial biofilms. Proceedings of the National Academy of Sciences of the United States of America 104(3):876-881.

Xia FH, Beyenal H, Lewandowski Z. 1998. An electrochemical technique to measure local flow velocity in biofilms. Water Research 32(12):3631-3636.

Zhang SF, Splendiani A, dos Santos LMF, Livingston AG. 1998. Determination of pollutant diffusion coefficients in naturally formed biofilms using a single tube extractive membrane bioreactor. Biotechnology and Bioengineering 59(1):80-89.

Zhang TC, Bishop PL. 1994. Evaluation of tortuosity factors and effective diffusivities in biofilms. Water Research 28(11):2279-2287.